STRUCTURAL CONTROLS ON THE CATALYTIC POLYMERIZATION OF HYDROQUINONE BY BIRNESSITES

MING-MING LIU, XING-HUI CAO, WEN-FENG TAN*, XIONG-HAN FENG, GUO-HONG QIU, XIU-HUA CHEN, AND FAN LIU

College of Resources and Environment, Huazhong Agricultural University, Wuhan 430070, P.R. China

Abstract—The role of Mn oxide in the abiotic formation of humic substances has been well demonstrated. However, information on the effect of crystal structure and surface-chemical characteristics of Mn oxide on this process is limited. In the present study, hexagonal and triclinic birnessites, synthesized in acidic and alkali media, were used to study the influence of the crystal-structure properties of birnessites on the oxidative polymerization of hydroquinone and to elucidate the catalytic mechanism of birnessites in the abiotic formation of humic-like polymers in hydroquinone-birnessite systems. The intermediate and final products formed in solution and solid-residue phases were identified by UV/Visible spectroscopy, atomic absorption spectrometry, Fourier-transform infrared spectroscopy, X-ray diffraction, solid-phase microextraction-gas chromatography-mass spectrometry, ion chromatography, and ultrafiltration. The degree of oxidative polymerization of hydroquinone was enhanced with increase in the interlayer hydrated H^+, the average oxidation state (AOS), and the specific surface area of birnessites. The nature of the functional groups of the humic-like polymers formed was, however, almost identical when hydroquinone was catalyzed by hexagonal and triclinic birnessites with similar AOS of Mn. The results indicated that crystal structure and surface-chemistry characteristics have significant influence on the oxidative activity of birnessites and the degree of polymerization of hydroquinone, but have little effect on the abiotic formation mechanism of humic-like polymers. The proposed oxidative polymerization pathway for hydroquinone is that, as it approaches the birnessite, it forms precursor surface complexes. As a strong oxidant, birnessite accepts an electron from hydroquinone, which is oxidized to 1,4-benzoquinone. The coupling, cleavage, polymerization, and decarboxylation reactions accompany the generation of 1,4-benzoquinone, lead to the release of CO_2 and carboxylic acid fragments, the generation of rhodochrosite, and the ultimate formation of humic-like polymers. These findings are of fundamental significance in understanding the catalytic role of birnessite and the mechanism for the abiotic formation of humic substances in nature.

Key Words—Birnessite, Catalytic Oxidation, Crystal Structure, Hydroquinone, Mn Oxide, Oxidative Polymerization.

INTRODUCTION

Humic substance (HS), a major constituent of soil organic matter, has attracted much attention from soil scientists because of its crucial role in agriculture and the environment (Wilson, 1991). The humification processes of organic molecules in soils and sediments are very complex and vary under different natural conditions, depending on the organic precursors (Shindo and Huang, 1982; Jokic *et al*., 2001b; Jokic *et al*., 2004) and catalysts (Kappler *et al*., 2000; Wang and Huang, 2000; Ahn *et al*., 2006) involved in the reaction systems.

Although the role of inorganic minerals in humification was recognized several decades ago (Scheffer *et al*., 1959), the abiotic formation of humic substances from organic precursors have often been ignored because abiotic processes are very difficult to distinguish from microbiological processes when they occur together (McBride, 1994; Ahn *et al*., 2006; Zavarzina, 2006). Moreover, the identification of the intermediate and final products is very difficult because they can be adsorbed easily on mineral surfaces which hampers the elucidation of the potential mechanisms of the humification processes. Research on the abiotic formation mechanism of humic substances has, therefore, become one of the most important, yet least understood, aspects of humus chemistry.

Many soil minerals, such as clay minerals, primary minerals, and aluminum, iron, and Mn (oxyhydr)oxides have been shown to have the ability to transform soil organic compounds into humic substances abiotically through their oxidative polymerization, ring cleavage, decarboxylation, and dealkylation (Shindo and Huang, 1985; Colarieti *et al*., 2006; Wang and Huang, 2000, 2003, 2005; Hardie *et al*., 2009a; Liu and Huang, 2002; Gonzalen and Laird, 2004; Bosetto *et al.*, 2002; Dec *et al*., 2001). Shindo and Huang (1985) studied the catalytic oxidative power of 14 soil minerals for the oxidative polymerization of hydroquinone. Of all the minerals investigated, Mn oxide was by far the most

effective oxidant, although the clay minerals mont-morillonite, vermiculite, illite, and kaolinite all had some effect. The strong catalytic oxidative activity of Mn oxide can be attributed to the following two points (Shindo and Huang, 1982): (1) Mn oxide, acting as a strong oxidant, catalyzed the oxidative polymerization of hydroquinone by accepting one or more electrons; (2) the degree of polymerization was enhanced by an increase in pH caused by reduction of the Mn oxide, due to deprotonation of hydroquinone with increasing pH. Therefore, Mn oxides were regarded as the most effective abiotic redox minerals found in soils and sediments.

Birnessite, a tetravalent Mn oxide commonly present in soil and sediments, is very effective at catalyzing the oxidative polymerization of the polyphenols (Wang and Huang, 1992), the Maillard reaction (Jokic, 2000; Jokic *et al.*, 2001b), and the integrated polyphenol-Maillard reaction (Jokic *et al.*, 2004; Wang and Huang, 2005), *etc.*, due to its low point of zero charge, large surface area, and strong acidic sites. Furthermore, Mn(IV) is more electronegative and has a greater oxidation potential than other metals, which also accounts for its strong catalytic power (Huang and Hardie, 2009). Birnessite has, therefore, become the most studied soil mineral in the field of abiotic formation of humic substances. Other studies have also focused on analyzing the effect of external environmental conditions, such as light (Jokic *et al.*, 2001a; Lee and Huang, 1995), temperature (Wang and Huang, 2003), pH value (Shindo and Huang, 1992), and oxygen (Wang and Huang, 2000) on the rate, degree, and products of the humification reaction. Jokic *et al.* (2001a) and Lee and Huang (1995) investigated the effect of light intensity on the catalytic activity of birnessite in promoting the Maillard reaction. Spectroscopic data showed that birnessite, in the presence of light, was a very active catalyst in the abiotic formation of humic substance in the glucose-glycine system. Birnessite also promoted the humification process even in the absence of light. The synergistic effects of the oxygen molecule and birnessite which played an important role in the abiotic transformation of pyrogallol were also observed by Wang and Huang (2000).

The effects of internal factors, such as the crystal-structure properties (crystal symmetry, average oxidation state (AOS), octahedral vacancies, and interlayer hydrated H$^+$) and the surface-chemistry characteristics of birnessite on the process and mechanism of the humification reaction are not well known. Previous research has shown that crystal-structure properties have significant effects on the adsorption, catalysis, and oxidation abilities of birnessite (Zhao *et al.*, 2009b; Tan *et al.*, 2009). For example, the amount of Cr(III) oxidation was affected markedly by the Mn AOS of birnessite (Kim *et al.*, 2002; Tan *et al.*, 2009), while the oxidation rates of Cr(III) (Nico and Zasoki, 2000) and

hydroquinone (Nico and Zasoki, 2001) were mainly controlled by the surface Mn(III) in birnessite. In addition, birnessite has two types of crystal symmetry: poorly crystallized hexagonal birnessite in acidic media (H-birnessite) and well crystallized triclinic birnessite in alkaline media (OH-birnessite). These different forms possess different chemical compositions, crystal-structure, and surface-chemical characteristics. Analysis of the effect of the crystal structure and surface-chemistry characteristics of birnessite on the oxidative polymerization process is crucial in understanding its catalytic role in the mechanism of abiotic formation of humic substance, and thus its environmental function in sequestration of soil organic carbon, mitigation of greenhouse gas emission, and in the global carbon cycle.

The purpose of the present study was to increase understanding of the role of Mn (oxyhydr)oxides in HS formation in natural systems. In the model system, several H- and OH-birnessites were synthesized with different AOS of Mn in acidic and alkaline media, and then they were used for the abiotic formation of hydroquinone-derived humic-like polymers. The degree of polymerization of hydroquinone and the amount of Mn^{2+} released to the solution phase from the various birnessites were investigated. The intermediate and final products formed during the abiotic, redox-driven poly-merization processes were characterized, the effect of crystal-structure properties on the redox polymerization processes was examined, and the mechanism for the catalytic role of birnessite in the abiotic formation of humic-like polymers was proposed.

MATERIALS AND METHODS

Sample preparation and characterization

H-birnessites were synthesized in an acidic medium according to procedures described by McKenzie (1971). A 300 mL sample of 0.667 mol L^{-1} KMnO$_4$ solution was heated and kept boiling at 110ºC in an oil bath under continuous stirring; then, 45 or 80 mL of 6 mol L^{-1} HCl was added dropwise to the KMnO$_4$ solution at a constant rate of 0.7 mL min^{-1}. After boiling for a further 30 min, the suspension was aged in an oven at 60ºC for 12 h, and then centrifuged at 25ºC at 25,000 × g in a Beckman super-speed refrigerated centrifuge. The product was washed with distilled deionized water, further purified by electro-dialysis at a voltage of 150−220 V until the conductivity of the supernatant was <20 S cm^{-1}, and then freeze dried. Based on the volume of HCl used, *i.e.* 45 or 80 mL, the synthetic H-birnessites were designated HB1 and HB2, respectively.

OH-birnessites were prepared in an alkaline medium according to Villalobos *et al.* (2003). 125 mL samples of 0.2018, 0.3026, and 0.5043 mol L^{-1} MnCl$_2$ solutions were each mixed thoroughly with 250 mL of 4.4 mol L^{-1} NaOH solution. Then, 125 mL of 0.2016 mol L^{-1} KMnO$_4$ was subsequently added dropwise at a rate of

0.7 mL min^{-1} under vigorous stirring to the pink Mn(OH)$_2$ gel precipitate formed above. After stirring for another 30 min, the products were aged in an oven at 60ºC for 12 h. The purification process was identical to that of H-birnessites. The products obtained were named OHB1, OHB2, and OHB3 and corresponded to the increasing concentrations of MnCl$_2$ used, respectively.

The crystal structures of the powder samples were characterized by X-ray diffraction (XRD) analysis, using a D8 Advance diffractometer (Bruker, Germany) with monochromatic CuKα radiation. The diffractometer was operated at a tube voltage of 40 kV and a tube current of 20 mA. The intensities were measured at a step-scanning rate of 0.02º per 0.5 s over a 2θ range of 5 to 85º. The AOS of Mn was measured by the oxalic acid-permanganate back-titration method (Kijima *et al.*, 2001). The specific surface area was measured by the BET method (N$_2$ adsorption) (Brunauer *et al.*, 1938) using an Autosorb-1 Surface Area Analyzer (Quantachrome, USA) after outgassing at 80ºC for 3 h.

Humic acid, used as a reference to compare the functional composition with that of the newly formed humic-like polymers, was purchased from Aldrich (Saint Louis, Missouri, USA) and purified according to the method described by Tan *et al.* (2008) except that the final treatment with Dowex 50W-X8 was not carried out. The purified Aldrich humic acid (PAHA) was then freeze dried and stored in a closed container placed in a desiccator. The molar mass of PAHA determined by viscometry and size exclusion chromatography was ~20 kDa, and the elemental composition (wt.%) on an ash-free basis was: C, 55.8%; O, 38.9%; H, 4.6%; N, 0.6%.

Incubation experiment

Majcher *et al.* (2000) compared the distribution of catechol-derived carbon in the solid, solution, and gas phases as a function of time during the oxidative polymerization of catechol as catalyzed by birnessite under both normal (unsterilized) and strictly sterile conditions. The results obtained were almost identical, which confirmed that the redox polymerization reaction under normal conditions was indeed abiotic, with very little influence from microorganisms. In the present work, the incubation experiments were, therefore, performed under normal conditions without strict sterilization except that the solutions were prepared with filter-sterilized, distilled-deionized water.

The abiotic, redox-driven polymerization reactions were carried out in several steps. First, 0.2750 g of hydroquinone was added to a 250 mL volumetric flask, diluted with 0.5 wt.% NaCl solution, and then adjusted to pH 7.0 using a few drops of 0.1 mol L^{-1} HCl or 0.1 mol L^{-1} NaOH. The final concentration of the hydroquinone solution was ~10.2 mmol L^{-1}. A 150 mL aliquot of this solution was then transferred to a 250 mL flask and sparged with nitrogen for 30 min. After that,

0.15 g of one of the various birnessites synthesized was added to this oxygen-free hydroquinone solution. Finally, the flasks were sealed tightly and the constituents allowed to react under vigorous stirring in a water bath at 25ºC for 1 min, 2 min, 3 min, 5 min, 8 min, 10 min, 30 min, 50 min, 100 min, 2 h, 3 h, 4 h, 5 h, 6 h, 10 h, 24 h, 48 h, 60 h, 72 h, or 3 months. After the selected reaction time, the suspension was centrifuged at 25,000 × g for 30 min to separate the solid residue from the supernatant.

Characterization of solid- and solution-phase reaction products

The supernatant obtained after different reaction times was filtered through a 0.45 μm polytetrafluoroethylene (PTFE) microporous filter. The solid residue was washed by repeated filtration with distilled-deionized water until the absorbance of the supernatant at 400 nm disappeared, and then centrifuged at 25,000 × g for 30 min. The supernatants from each washing step were collected and added to the initial centrifugal supernatant. The total centrifugal supernatant was acidified to pH 1.0 using 6 mol L^{-1} HCl, and allowed to stand for 24 h to precipitate the humic-like polymers (Hardie *et al.*, 2007). The acidified suspensions were then centrifuged at 12,000 × g for 40 min to separate the humic-like polymers precipitated from the solution phase. The humic-like polymer fractions were washed and purified with distilled-deionized water, and then freeze dried.

Absorbance properties of the humic-like polymers formed

The yield of humic acid is typically related to the extent of absorbance at 400 and 600 nm (Shindo and Huang, 1982); therefore, in the present study, the absorbance at 400 nm was recorded as an indication of the degree of oxidative polymerization of hydroquinone.

Identification of the intermediate and final reaction products

The amount of Mn^{2+} released to the solution was determined using atomic absorption spectroscopy (Varian AA240FS, Palo Alto, California, USA). The solid residue was freeze dried and analyzed by XRD to examine the change in crystal structure after different reaction times.

The non-polar to medium-polar intermediates formed during the oxidative polymerization process were determined by solid-phase micro-extraction (SPME) combined with gas chromatography (GC) or gas chromatography-mass spectrometry (GC-MS), using a homemade SPME device with a sol-gel-derived butyl methacrylate–hydroxy-terminated silicone oil (BMA−OH-TSO) fiber (Liu *et al.*, 2005). The GC analyses were carried out on a SP-6890 capillary GC system (Shandong Lunan Ruihong Chemical Instrument

Corporation, Shandong, China) equipped with a capillary split/splitless injector and flame ionization detector (FID). The GC-MS analyses were performed on a GC tandem MS instrument (CP-3800-Saturn 2200, Varian, Walnut Creek, California, USA). The SPME operation procedure can be described as follows: a 5 mL aliquot of the suspension filtered through a 0.45 μm PTFE microporous filter was pipetted with a micropipettor into a 12 mL glass vial containing a magnetic stirring bar and 2 g of NaCl. To avoid sample evaporation loss, the vial was sealed tightly with a butyl rubber stopper wrapped with polytetrafluoroethylene sealing tape and an aluminum cap. Afterward, the stainless steel needle, where the fiber was housed, was pushed through the vial septum, and then the fiber was pushed out of the housing and introduced to the headspace of the sample solution, which was then placed in a constant-temperature water bath at 25ºC and stirred continuously with a magnetic stirrer for 20 min. After extraction, the fiber was removed from the sample vial and inserted immediately into the heated GC injector for a 5 min desorption time. The GC conditions were as follows: the injector temperature was 250ºC, the FID temperature was 300ºC, and the oven temperature was maintained at 60ºC for 2 min, programmed to then increase at 10ºC min^{-1} to 280ºC, and held there for a further 10 min. The strong polar carboxylic acid intermediates formed during the oxidative polymerization process were examined by ion chromatography (Dionex ICS-1000, Sunnyvale, California, USA). The eluent used for the separation of carboxylic acids was 0.9 mmol L^{-1} Na$_2$CO$_3$−0.85 mmol L^{-1} NaHCO$_3$ solution, and the elution rate was 2 mL min^{-1}.

Fourier-transform infrared spectroscopy (FTIR) spectra of the humic-like polymers formed

The humic-like polymers formed were partially precipitated as solid residues, and partially dissolved in the solution phase. Humic-like polymers precipitated as solid residues have larger molecular weights, which may be more like the unpurified Aldrich Humic Acid (AHA). Humic-like polymers dissolved in the solution phase have smaller molecular weights, and can be precipitated from the centrifugal supernatant by 6 mol L^{-1} HCl. These are more like the purified AHA. In order to verify that the hydroquinone-derived humic-like polymers obtained in this work had similar functional groups to those of the natural humic acid, the FTIR spectra of the solid residues were compared with those of the unpurified AHA, and those of the acidic precipitated humic-like polymers with the purified AHA. The FTIR spectra of these samples were obtained using an Avatar 330 FTIR spectrometer (Thermo Nicolet, Madison, Wisconsin, USA) by grinding the solid residue and blending it 1:100 (wt.:wt.) with KBr, using a pure KBr pellet in air as background, with a resolution of 4 cm^{-1} over the full mid-IR range (4000−400 cm^{-1}).

Molecular-size distribution of the humic-like polymers precipitated from the centrifugal supernatant

The mass distribution of the humic-like polymer fractions precipitated from the centrifugal supernatant by 6 mol L^{-1} HCl was measured using a cross-flow ultrafiltration technique (MinitanTM, Millipore) (Kilduff and Weber, 1992; Li *et al.*, 2004). The hydrophilic cellulose membranes used had nominal molecular weight cut-off values of 3, 10, and 30 kDa (Ultracel-PL, Millipore). A working solution of the humic-like polymer fractions at 600 mg L^{-1} was prepared by dissolving an appropriate amount of the humic-like polymers extracted by acidic precipitation into a buffer solution containing 10 mmol L^{-1} NaCl, 1 mmol L^{-1} sodium phosphate, and 10 mmol L^{-1} NaN$_3$. The ultrafiltration process was performed at a flow rate of 300 mL min^{-1} with a combined diafiltration and concentration method described by Kilduff and Weber (1992) and Li *et al.* (2004). The four humic-like polymer fractions obtained from this procedure were labeled UF1 (<3 kDa), UF2 (3-10 kDa), UF3 (10−30 kDa), and UF4 (>30 kDa), respectively. Although the ultrafiltration technique is a simple and effective method for the analysis of the molecular-size distribution of the humic-like polymers formed, the experimental error is relatively large if aggregation occurs during drying because this will lead to incomplete dispersion of the humic-like polymers in solution.

To ensure the reliability of the analytical results, each incubation/characterization experiment was carried out in duplicate. The quantification of Mn^{2+} and other low-molecular-weight intermediate and final products, such as 1,4-benzoquinone and formic acid, was performed by the external standard method (Liu *et al.*, 2005). The error in terms of duplicate experiments/measurements was always <5%. Error bars are not shown explicitly in the figures.

RESULTS

Characterization of the synthetic birnessites

The powder XRD patterns of the synthetic HB and OHB minerals showed that each birnessite was pure (Figure 1). The HB series were characterized by four peaks at 0.732, 0.364, 0.245, and 0.142 nm, and the OHB series by five peaks at 0.724, 0.363, 0.245, 0.237, and 0.142 nm. These results agree well with JCPDS 23-1239 (hexagonal crystal symmetry) and 23-1046 (monoclinic crystal symmetry), respectively. The basic properties of the HB and OHB minerals tested (Table 1) revealed that the AOS values of Mn for HB1 and HB2 were 4.0 and 3.67, and for OHB1, OHB2, and OHB3 were 3.97, 3.75, and 3.55, respectively. The specific surface area of the HB samples decreased with increasing AOS of Mn, while that of the OHB samples increased with increasing AOS of Mn, giving specific values of 15.9 and
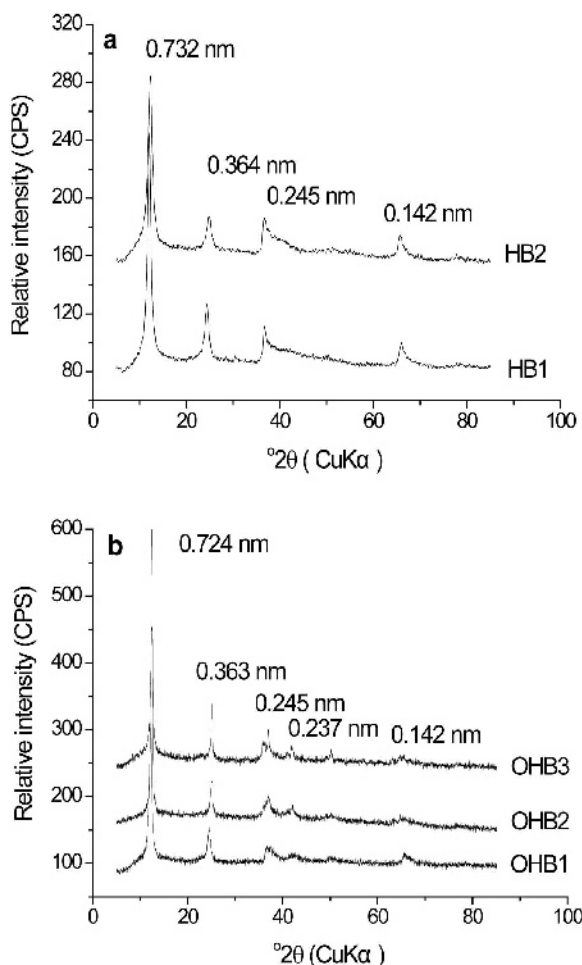
Figure 1. Powder XRD patterns of the synthetic HB (a) and OHB (b) samples.

Table 1. The average AOS values of Mn and the specific surface areas of the HB and OHB samples.

Birnessite samples	AOS of Mn	Specific surface area ($m^2 \, g^{-1}$)
HB1	4.00	15.9
HB2	3.67	98.6
OHB1	3.97	79.6
OHB2	3.75	77.0
OHB3	3.55	69.7

system was much greater than that observed in the hydroquinone-OHB system. For the same type of birnessites, the equilibrium absorbance decreased slightly with a decrease in AOS of Mn. The final pH of the reaction system changed from 7.0 to ~8.0 after 72 h of redox polymerization reaction between hydroquinone and the HB or OHB minerals.

Identification of the intermediate and final reaction products

The amount of Mn^{2+} released to the solution during the oxidative polymerization of hydroquinone, as catalyzed by HB and OHB minerals, decreased as the AOS of Mn increased (Figure 3). This can be explained by the fact that the Mn content in birnessite decreases as the AOS of Mn increases (Zhao *et al*., 2009b). The final concentration of Mn^{2+} in the supernatant was ~4.0–4.8 mmol L^{-1}, indicating that only a small proportion of Mn^{2+} was released to the solution phase. This is mainly because Mn^{2+} is partially adsorbed by the humic-like polymers formed or precipitated with CO_2 to form rhodochrosite (Hardie, 2008).

The XRD patterns (Figure 4) of the solid residues after different reaction times between hydroquinone and HB1 revealed that the characteristic peaks of H-birnessites (0.721, 0.361, 0.246, and 0.142 nm) disappeared gradually with reaction time. In contrast, peaks characteristic of crystalline $MnCO_3$ (rhodochrosite, JCPDS No. 7-268) at 0.369, 0.285, 0.239, 0.217, 0.201, and 0.177 nm appeared and became stronger. The birnessite added was transformed almost completely to rhodochrosite after 5 days. This was attributed mainly to the reaction between CO_2 derived from the cleavage polymerization of hydroquinone and Mn^{2+} released from the birnessite to the solution (Hardie *et al*., 2007; Hardie, 2008).

1,4-benzoquinone was the only product detected by the SPME-GC and SPME-GC-MS methods during the initial reaction period of hydroquinone polymerization catalyzed by HB1. The amount of 1,4-benzoquinone increased rapidly (Figure 5) to a maximum of 8.1 mmol L^{-1} after 2 min. From 2 min to 30 min, the amount decreased sharply, at which time no further 1,4-benzoquinone was detected. The maximum amount of 1,4-benzoquinone was equivalent to 80% of the hydroquinone added to the

98.6 $m^2 \, g^{-1}$ for HB1 and HB2, respectively, and 79.6, 77.0, and 69.7 $m^2 \, g^{-1}$ for OHB1, OHB2, and OHB3, respectively. The H-birnessite with high AOS of Mn contains a large number of surface OH groups (Zhao *et al*., 2009a). The strong hydrogen bonding interaction with the surface OH groups will lead to the agglomeration of birnessite particles. This may account for the surface area of HB1 being much smaller than that of HB2, which has a smaller AOS of Mn (Zhao *et al*., 2009a).

Characterization of solid- and solution-phase reaction products

Absorbance properties of the humic-like polymers formed. The formation of the humic-like polymers in the solution phase during the oxidative polymerization of hydroquinone, as catalyzed by the synthetic HB and OHB minerals, increased with reaction time (Figure 2), reaching steady state after ~60 h for the OHB series and ~96 h for the HB series. Moreover, the steady absorbance value obtained in the hydroquinone-HB
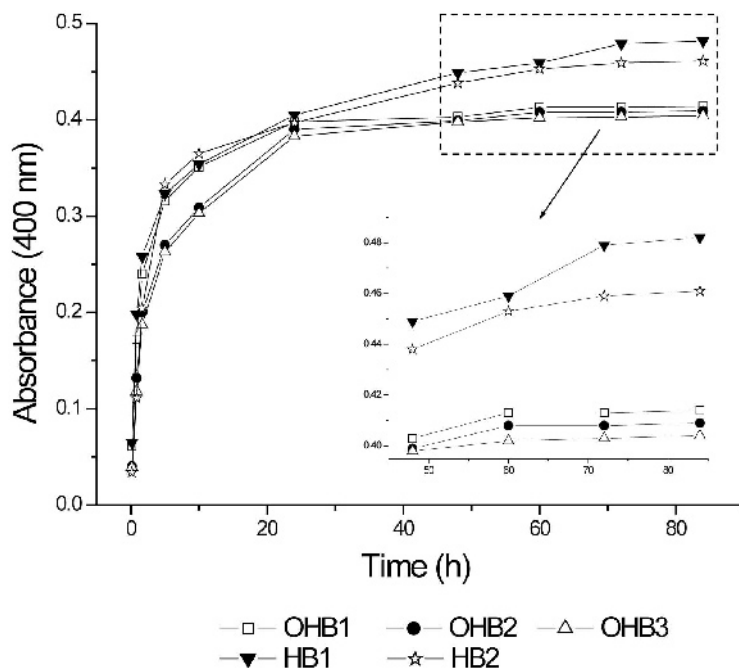
Figure 2. Formation of humic-like polymers in the solution phase during the oxidative polymerization of hydroquinone as catalyzed by synthetic HB and OHB minerals.

reaction system, indicating that 1,4-benzoquinone was probably the major intermediate of the oxidative polymerization of hydroquinone.

Formic acid was also found (using ion chromatography) throughout the reaction, indicating that the generation of 1,4-benzoquinone was accompanied by an

almost immediate opening of the ring to yield formic acid. The amount of formic acid released to the solution during the HB1-catalyzed oxidative polymerization of hydroquinone was enhanced with increasing reaction time, and reached a plateau of 0.85 mmol L^{-1} within 24 h (Figure 5).
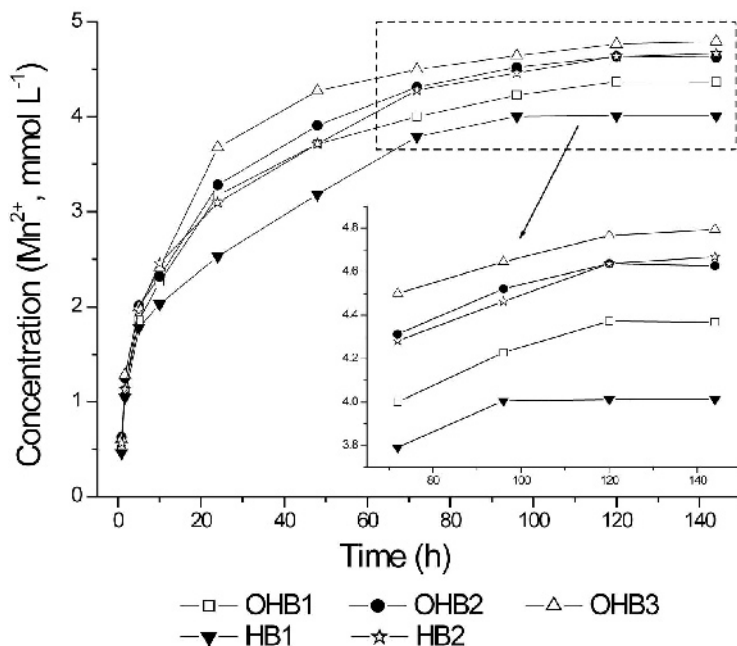

Figure 3. Release of Mn^{2+} to the solution phase during the oxidative polymerization of hydroquinone as catalyzed by synthetic HB and OHB minerals.
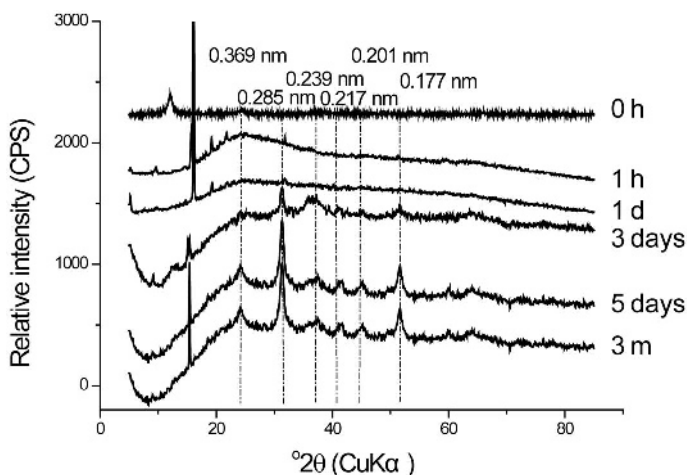
Figure 4. XRD patterns of the solid residue separated from suspension by centrifugation after different reaction times between hydroquinone and HB1.

FTIR spectra of the humic-like polymers formed

The FTIR spectra of the solid residues separated from the suspension by centrifugation after different reaction times between hydroquinone and HB1 were compared with those of the unreacted HB1 and the unpurified AHA (Figure 6). Compared with the FTIR spectrum of HB1, the intensities of the absorption bands characteristic of birnessite Mn-O vibrations, at 451 and 511 cm^{-1} (Potter and Rossman, 1979), decreased markedly in the reacted solid residues as the reaction time was prolonged, due to the reduction of birnessite and the release of Mn^{2+} to solution. The FTIR absorption bands of the solid residues were also very similar to those of the unpurified AHA, suggesting that the polymerization of hydroquinone occurred under the catalytic oxidation of birnessite, leading to the abiotic formation of humic-like polymers.

The functional groups in these humic-like products included aromatic rings (1621 cm^{-1}) and hydroxyl (3421 cm^{-1}), carboxyl (1581cm^{-1}, 1384 cm^{-1}), methyl (2972 cm^{-1}), and methylene (2923 cm^{-1}) groups (Hardie, 2008). The absorption frequency of C=C aromatic stretching modes shifted gradually from 1632 to 1620 cm^{-1} with increasing reaction time, suggesting a greater degree of aromatic condensation in the humic-like products as reaction times increased. The carboxyl groups were predominantly deprotonated, as indicated by symmetric (1581 cm^{-1}) and anti-symmetric (1384 cm^{-1}) COO$^-$ stretching bands. The absence of an absorption band at ~1710 cm^{-1} (undissociated carboxyl) can be attributed to the increased pH from 7 to 8 at the end of the reaction (Jokic, 2000). Owing to the intramolecular H-bonding interaction, the hydroxyl
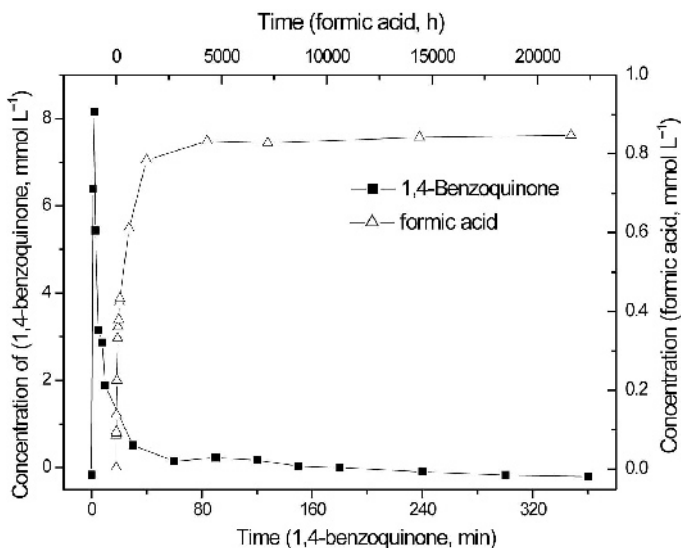

Figure 5. 1,4-benzoquinone and formic acid released to solution during HB-catalyzed oxidative polymerization of hydroquinone.
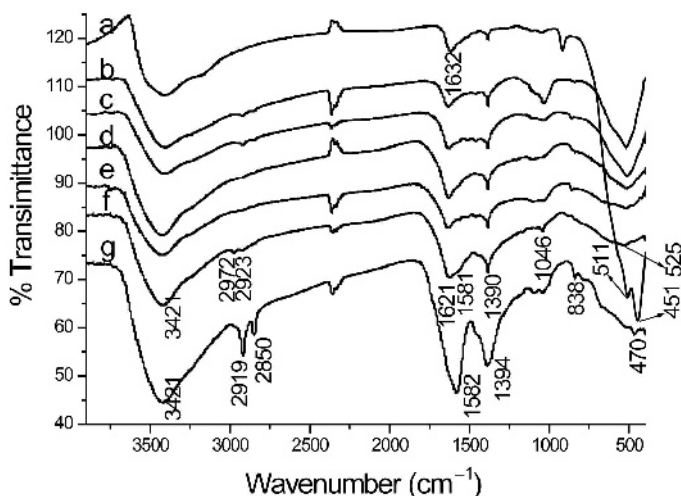
Figure 6. FTIR spectra of (a) HB1; solid residues separated from the solution phase after reaction of HB1 with hydroquinone for (b) 1 h, (c) 1 day, (d) 5 days, (e) 8 days, and (f) 3 months; and (g) unpurified AHA.

groups in the humic-like products were clearly in an associated form (3200−3400 cm^{-1}) rather than vibrating freely (3610−3670 cm^{-1}) (Aktas *et al.*, 2003).

The FTIR spectra of the humic-like polymer fractions precipitated from the centrifugal supernatant by 6 mol L^{-1} HCl after different reaction times between hydroquinone and HB1 were compared with that of PAHA (Figure 7). The spectra were similar, except that the intensities of the absorption bands at 2918 and 2845 cm^{-1} (C–H stretch of methyl and methylene) from the humic-like polymers were much less than those of PAHA. This result further confirmed the oxidative polymerization of hydroquinone and the abiotic formation of humic-like polymers in the hydroquinone-birnessite system. In comparison with the FTIR spec-

trum of the separated solid residue (Figure 6), several new absorption peaks were observed, at 1711, 1498, 1447, 1223, and 860 cm^{-1} in the extracted humic-like polymers after different reaction times. The presence of the characteristic absorption bands of the undissociated carboxyl group at 1711 cm^{-1} (symmetric carboxyl C=O stretch of COOH) and phenoxyl group at 1223 cm^{-1} (C−O stretch of phenol or phenyl ethers) was attributed to the strong acidic conditions (pH 1) used for the extraction of the polymer. The absorption bands at 1617, 1498, 1447, and 860 cm^{-1} were ascribed to the C=C stretch and C−H bending vibrations of aromatic rings. These observations (Figure 7) showed clearly that the intensity of the absorption band at 1617 cm^{-1} was strengthened while the bands at 1498, 1447, and
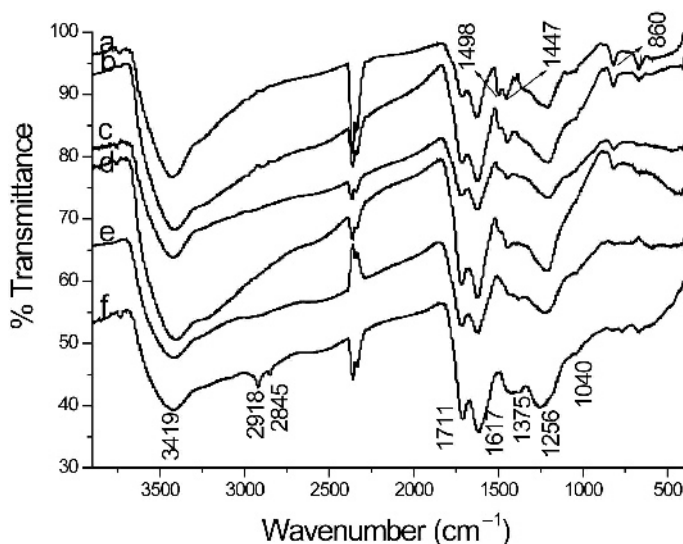

Figure 7. FTIR spectra of humic-like polymer fractions extracted from the centrifugal supernatant by 6 mol L^{-1} HCl after reaction of HB1 with hydroquinone for (a) 1 h, (b) 1 day, (c) 5 days, (d) 8 days, and (e) 3 months and (f) PAHA.
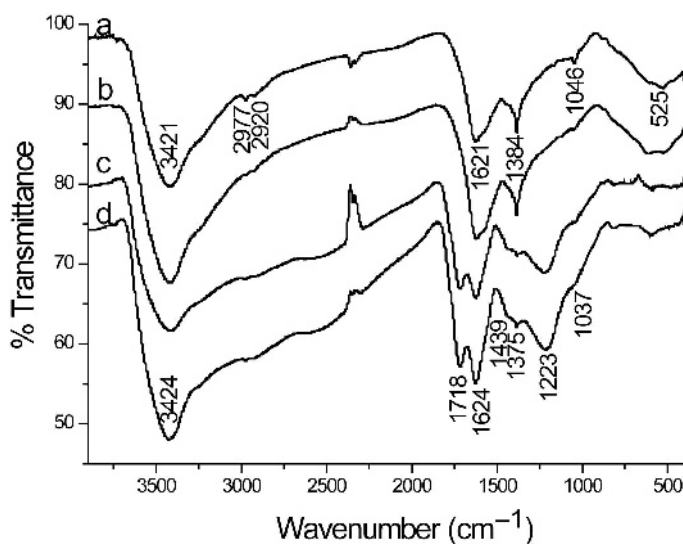
Figure 8. FTIR spectra of the solid residues separated from the reaction system and the humic-like polymer fractions extracted from the centrifugal supernatant by 6 mol L^{-1} HCl after 3 months of oxidative polymerization of hydroquinone by HB1 and OHB1. (a) The solid residues obtained in the hydroquinone-HB1 system; (b) the solid residues obtained in the hydroquinone-OHB1 system; (c) the humic-like polymer fractions obtained in the hydroquinone-HB1 system; (d) the humic-like polymer fractions obtained in the hydroquinone-OHB1 system.

860 cm^{-1} weakened with increasing degrees of aromatic condensation.

After 3 months of oxidative polymerization of hydroquinone by HB1 and OHB1, the FTIR spectra of the humic-like products were almost identical (Figure 8), indicating that the crystal structure properties of birnessites did not have a significant influence on the nature of functional groups of the humic-like products and, thus, on the oxidative polymerization mechanism of hydroquinone. Therefore, only HB1 was selected for subsequent characterization experiments of the intermediate and final reaction products, and was assumed to represent the expected behavior of the other birnessites.

Molecular-size distribution of the humic-like polymers precipitated from the centrifugal supernatant

The average molecular weight of the four humic-like polymers formed and extracted by the ultrafiltration technique was relatively large at >30 kDa (Table 2), and accounted for 75.7 wt.% of the total humic-like polymers in UF4. These results are consistent with those of Li *et al.* (2004).

DISCUSSION

Influence of crystal-structure properties on the abiotic oxidative polymerization of hydroquinone

The H-birnessites have a greater oxidation capacity than the OH-birnessites (Figure 2). Even though the same crystal symmetry is assigned to both forms, the larger the AOS of Mn, the greater the oxidation capacity. The differences in oxidation capacity between these birnessites were mainly attributed to their different

crystal-structure and surface-chemical characteristics: H-birnessite has hexagonal layer symmetry with layers comprising edge-sharing Mn(IV)O$_6$ octahedra, Mn(III)O$_6$ octahedra, and vacant octahedral sites (Villalobos *et al.*, 2006). These layers are separated from one another by hydrated interlayer cations Mn^{2+}, Mn(III) OH^{2+}, K$^+$, H$^+$, *etc.*, which are located above or below vacant octahedral sites (Villalobos *et al.*, 2006; Lanson *et al.*, 2000). If the AOS of Mn is high, H$^+$ will become the predominant interlayer cation because H-birnessite is synthesized in a strong acidic medium (Zhao *et al.*, 2009a). OH-birnessite has a layered structure with monoclinic symmetry. Within the MnO$_6$ octahedral sheets, rows rich in Mn(III) parallel to the *b* axis are separated from one another along the *a* axis by two Mn(IV) rows (Lanson *et al.*, 2002). The migration and disporportionation of Mn(III) lead to the generation of a small quantity of vacant octahedral sites and Mn(II) in the OH-birnessite (Drits *et al.*, 1997).

The two H-birnessites exhibited greater oxidation capacities than the three OH-birnessites which can be

Table 2. Mass distribution of humic-like polymer fractions extracted by ultrafiltration from the centrifugal supernatant after 3 months of reaction between hydroquinone and HB1.

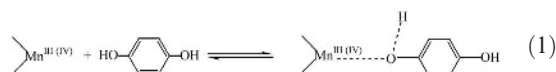| Humic-like polymer fractions	Molecular weight cutoffs	Mass distribution (wt.%)
UF1	<3 kDa	19.67
UF2	3−10 kDa	0.33
UF3	10−30 kDa	4.33
UF4	>30 kDa	75.67

explained by the fact that H-birnessites have more hydrated H^+ in the interlayers than OH-birnessites (Zhao *et al.*, 2009a). H-birnessites can, therefore, provide more protons to react with basic sites such as surface oxygens of the birnessite, thus accelerating the release of OH groups into solution, leading to an increase in pH and further oxidation polymerization of hydroquinone. For birnessites belonging to the same crystal symmetry, the larger the AOS of Mn, the greater the oxidation capacity. This is because: (1) birnessites with greater AOS values of Mn have more Mn(IV) and less Mn(III) in the octahedral sheets, and so they can accept more electrons from hydroquinone, leading to greater oxidation capacities; and (2) the number of vacant octahedral sites increases with increasing AOS values of Mn (Zhao *et al.*, 2009b). To make up for the excess negative layer charge, more interlayer hydrated H^+ will locate above or below the vacant octahedral sites, leading to a stronger Bronsted acidity. The vacant sites can, therefore, attract more protons to the surface oxygens of the birnessite structure and, thereby, enhance the catalytic oxidative power of birnessite. Although HB2 (3.67) has smaller AOS values of Mn than OHB1 (3.97), its oxidation capacity is larger. A possible reason is that the former has a larger surface area than the latter, which can provide more surface sites for birnessite to form precursor surface complexes. On the whole, the oxidation activity of birnessites is mainly influenced by the interlayer hydrated H^+, the AOS of Mn, and the specific surface area.

Oxidative polymerization pathway of hydroquinone as catalyzed by birnessite

The catalytic oxidative activity of birnessite is a function of its ability to act as proton donor or electron acceptor (Jokic, 2000). Mn(IV) and Mn(III) on the exposed edges of birnessite act as oxidative sites that accept an electron pair from hydroquinone (Stone, 1987). When Mn replaces H in hydroquinone to form metal-hydroquinone complexes, the electron cloud delocalizes from phenolic oxygen into the π-orbital formed from overlap of the 2p orbitals of the aromatic C atoms, thus accelerating the formation of semiquinone free radicals and their coupling to form polycondensates (Liu and Huang, 2002; Matocha *et al.*, 2001). The interlayer hydrated H^+, bonded to the lattice oxygens, serve as hard Bronsted acid sites. When Mn(IV) or Mn(III) accepts electrons from hydroquinone, the dehydroxylation of birnessite occurs simultaneously with the reduction of high-valence Mn, leading to an increase in the solution pH (Bartlett and Ross, 2005). The increased pH promotes the deprotonation of hydroquinone, and further drives the redox polymerization reaction between hydroquinone and birnessite (Shindo and Huang, 1982). The synergistic effect of high-valence Mn on the edges and the hydrated H^+ in the interlayer leads to the final decomposition of birnessite
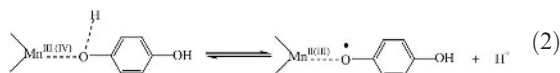
and the abiotic formation of humic-like polymers. The following mechanism is proposed for the oxidative polymerization pathways of hydroquinone as catalyzed by birnessite, according to the intermediate and final products detected in the solution and solid-residue phases, such as 1,4-benzoquinone, formic acid, and rhodochrosite:

(1) Hydroquinone approaches the surface of birnessite to form a precursor complex with Mn(IV) and Mn(III) on the exposed edges of birnessite (Stone, 1987; Matocha *et al.*, 2001) (equation 1):

$$\text{>Mn}^{III(IV)} + HO-\langle\!\!\!\bigcirc\!\!\!\rangle-OH \rightleftharpoons \text{>Mn}^{III(IV)}\cdots O-\langle\!\!\!\bigcirc\!\!\!\rangle-OH \quad (1)$$
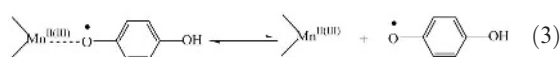
where > represents chemical bonds between edge-surface Mn(III) or Mn(IV) centers and the lattice oxygens.

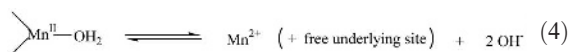(2) Electron transfer between Mn-hydroquinone complexes (equation 2):

$$\text{>Mn}^{III(IV)}\cdots O-\langle\!\!\!\bigcirc\!\!\!\rangle-OH \rightleftharpoons \text{>Mn}^{II(III)}\cdots \overset{\bullet}{O}-\langle\!\!\!\bigcirc\!\!\!\rangle-OH + H^+ \quad (2)$$

(3) Release of semiquinone radical intermediate (equation 3):

$$\text{>Mn}^{II(III)}\cdots \overset{\bullet}{O}-\langle\!\!\!\bigcirc\!\!\!\rangle-OH \longrightarrow \text{>Mn}^{II(III)} + \overset{\bullet}{O}-\langle\!\!\!\bigcirc\!\!\!\rangle-OH \quad (3)$$

(4) Release of reduced Mn^{2+} into solution and the dehydroxylation of birnessite (equation 4):

$$\text{>Mn}^{II}-OH_2 \rightleftharpoons Mn^{2+} \; (+ \text{free underlying site}) + 2\,OH^- \quad (4)$$

The Mn(III) reduced from Mn(IV) accepts another electron from hydroquinone or the semiquinone radical, and then transforms to Mn(II) and releases the reduced Mn^{2+} to solution.

(5) The semiquinone radical undergoes further complexation and subsequent electron transfer reaction with Mn(IV) or Mn(III) on the edge of birnessite, leading to the generation of the 1,4-benzoquinone radical (equation 5) (Matocha *et al.*, 2001).

$$\text{>Mn}^{II(III)}\cdots \overset{\bullet}{O}-\langle\!\!\!\bigcirc\!\!\!\rangle-\overset{\bullet}{O} \rightleftharpoons \text{>Mn}^{II(III)} + \overset{\bullet}{O}-\langle\!\!\!\bigcirc\!\!\!\rangle-\overset{\bullet}{O} \quad (5)$$

(6) The coupling, cleavage, and polymerization reactions: the 1,4-benzoquinone radical has very strong reactivity. The proposed oxidative polymerization processes of 1,4-benzoquinone radical are as follows (Figure 9): (i) The configurational transition of 1,4-benzoquinone radical can give rise to the production of 1,4-benzoquinone. (ii) The dimer and polymer of 1,4-benzoquinone can be formed by the coupling of 1,4-benzoquinone radical. (iii) The ring cleavage of 1,4-benzoquinone can occur simultaneously with the
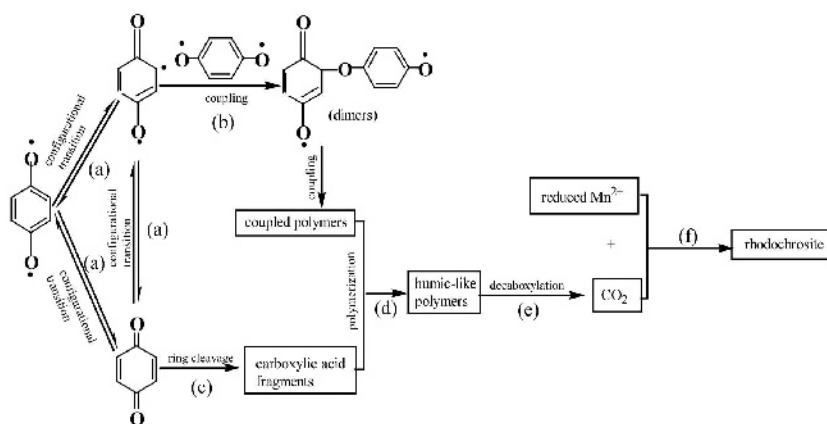
Figure 9. The proposed oxidative polymerization processes of the 1,4-benquinone radical.

generation of 1,4-benzoquinone, leading to partial transformation of hydroquinone to carboxylic acid fragments (Liu and Huang, 2001). (iv) The humic-like polymers can be formed through the polymerization of the carboxylic acid fractions generated and the coupled polymers of the 1,4-benzoquinone radical. (v) The decarboxylation reaction also brings about partial release of CO_2 from the humic-like polymer formed. (vi) The generation of rhodochrosite is caused by the combination reaction between CO_2 and the liberated Mn^{2+} (Hardie *et al.*, 2007, 2009a, 2009b), which is of fundamental significance in understanding the formation mechanism of $MnCO_3$ in natural environments.

CONCLUSIONS

Although birnessites synthesized under experimental conditions are somewhat different from those found in natural soils, they can be used as models to elucidate the influence of variable crystal structure on oxidative polymerization processes, considering that the incubation experiments are difficult to perform on soil birnessites. In the present study the crystal-structure properties of birnessites and their surface-chemical properties significantly influenced the oxidative activity of birnessites and the degree of polymerization of hydroquinone; however, their effect on the functional composition of the humic-like products formed and the oxidative polymerization pathway of hydroquinone were insignificant. H-birnessite exhibited a greater oxidation capacity than OH-birnessite because H-birnessite has more hydrated H^+ in the interlayers, while in birnessites of the same crystal symmetry, the greater the AOS of Mn, the greater the oxidation capacities and the smaller the amount of Mn^{2+} released. The present findings explain why different studies have obtained different results for the catalytic oxidative activity of birnessites in promoting the abiotic transformation of organic molecules and subsequent formation of humic substances.

The proposed oxidative polymerization pathway of hydroquinone as catalyzed by birnessite is as follows: hydroquinone as a reductant provides an electron for Mn(IV) or Mn(III) on the exposed edges of birnessites, and then is oxidized to 1,4-benzoquinone. The coupling, cleavage, polymerization, and decarboxylation reactions occur simultaneously with the generation of 1,4-benzoquinone, leading to (1) the formation of coupled polymer of 1,4-benzoquinone, (2) the release of carboxylic acid fragments and CO_2, and (3) the ultimate formation of humic-like polymers. Mn^{2+} liberated from the birnessite is precipitated with the CO_2 released to form rhodochrosite. Results from the present study suggest that the birnessite-induced abiotic polymerization mechanism may play a significant role in the formation of more complex organic compounds in soil, particularly under neutral to alkaline conditions. The results also provide experimental support for the hypothesis of the polyphenol-induced formation of rhodochrosite in wetlands as a result of the abiotic redox polymerization of hydroquinone as catalyzed by birnessites.

ACKNOWLEDGMENTS

REFERENCES

Ahn, M.-Y., Martinez, C.E., Archibald, D.D., Zimmerman, A.R., Bollag, J.-M., and Dec, J. (2006) Transformation of catechol in the presence of a laccase and birnessite. *Soil Biology & Biochemistry*, **38**, 1015−1020.

Aktas, N., Sahiner, N., Kantoglu, O., Salih, B., and Tanyolac, A. (2003) Biosynthesis and characterization of laccase catalyzed poly(catechol). *Journal of Polymers and ther Environment*, **11**, 123−128.

Bartlett, R.J. and Ross, D.S. (2005) Chemistry of redox processes in soils. Pp. 461−487 in: *Chemical Processes in Soils* (M.A. Tabatabai, D.L. Sparks, L. Al-Amoodi, and

W.A. Dick, editors). Soil Science Society of America, Madison, Wisconsin, USA.

Bosetto, M., Arfaioli, P., and Pantani, O.L. (2002) Study of the Maillard reaction products formed by glycine and D-glucose on different mineral substrates. *Clay Minerals*, **37**, 195–204.

Brunauer, S., Emmett, P.H., and Teller, E. (1938) Adsorption of gases in multi molecular layers. *Journal of the American Chemical Society*, **60**, 309–319.

Colarieti, M.L., Toscano, G., Ardi, M.R., and Greco, Jr. G. (2006) Abiotic oxidation of catechol by soil metal oxides. *Journal of Hazardous Materials*, **134**, 161–168.

Dec, J., Haider, K., and Bollag, J. (2001) Decarboxylation and demethoxylation of naturally occurring phenols during coupling reactions and polymerization. *Soil Science*, **166**, 660–671.

Drits, V.A., Silvester, E., Gorshkov, A.I., and Manceau, A. (1997) Structure of synthetic monoclinic Na-rich birnessite and hexagonal birnessite: I. Results from X-ray diffraction and selected-area electron diffraction. *Amercian Mineralogist*, **82**, 946–961.

Gonzalen, J.M. and Laird, D.A. (2004) Role of smectites and Al-substituted goethites in the catalytic condensation of arginine and glucose. *Clays and Clay Minerals*, **52**, 443–450.

Hardie, A.G. (2008) Pathways of abiotic humification as catalyzed by mineral colloids. PhD thesis, University of Saskatchewan, Saskatoon, Canada, 255 pp.

Hardie, A.G., Dynes, J.J., Kozak, L.M., and Huang, P.M. (2007) Influence of polyphenols on the intergrated polyphenol-Maillard reaction humification pathway as catalyzed by birnessite. *Annals of Environmental Science*, **1**, 91–110.

Hardie, A.G., Dynes, J.J., Kozak, L.M., and Huang, P.M. (2009a) The role of glucose in abiotic humification pathways as catalyzed by birnessite. *Journal of Molecular Catalysis A − Chemical*, **308**, 114–126.

Hardie, A.G., Dynes, J.J., Kozak, L.M., and Huang, P.M. (2009b) Biomolecule-induced carbonate genesis in abiotic formation of humic substances in nature. *Canadian Journal of Soil Science*, **89**, 445–453.

Huang, P.M. and Hardie, A.G. (2009) Formation mechanisms of humic substances in the environment. Pp. 41–109 in: *Biophysico-chemical Processes Involving Nonliving Natural Organic Matter in the Environment. Vol. 2* (N. Senesi, B. Xing and P.M. Huang, editors). Wiley-IUPAC series Biophysico-Chemical Processes in Environmental Systems. John Wiley & Sons, Hoboken, New Jersey, USA.

Jokic, A. (2000) The catalytic role of birnessite in the Maillard reaction and the abiotic formation of humic substances. PhD thesis, University of Saskatchewan, Saskatoon, Canada, 184 pp.

Jokic, A., Frenkel, A.I., and Huang, P.M. (2001a) Effect of light on birnessite catalysis of the Maillard reaction and its implication in humification. *Canadian Journal of Soil Science*, **81**, 277–283.

Jokic, A., Frenkel, A.I., Vairavamurthy, M.A., and Huang, P.M. (2001b) Birnessite catalysis of the Maillard reaction: its significance in natural humification. *Geophysical Research Letters*, **28**, 3899–3902.

Jokic, A., Wang, M.C., Liu, C., Frenkel, A.I., and Huang, P.M. (2004) Integration of the polyphenol and Maillard reactions into a unified abiotic pathway for humification in nature: the role of δ-MnO$_2$. *Organic Geochemistry*, **35**, 747–762.

Kappler, A., Ji, R., and Brune, A. (2000) Synthesis and characterization of specifically ^{14}C-labeled humic model compounds for feeding trials with soil-feeding termites. *Soil Biology & Biochemistry*, **32**, 1271–1280.

Kijima, N., Yasuda, H., Sato, T., and Yoshimura, Y. (2001) Preparation and characterization of open tunnel oxide α-MnO$_2$ precipitated by ozone oxidation. *Journal of Solid State Chemistry*, **159**, 94–102.

Kilduff, J.E. and Weber, W.J. (1992) Transport and separation of organic macromolecules in ultrafiltration processes. *Environmental Science & Technology*, **26**, 569–577.

Kim, J.B., Dixon, J.B., and Chusuei, C.C. (2002) Oxidation of chromium(III) to (VI) by manganese oxides. *Soil Science Society of America Journal*, **66**, 306–315.

Lanson, B., Drits, V.A., Silvester, E., and Manceau, A. (2000) Structure of H-exchanged hexagonal birnessite and its mechanism of formation from Na-rich monoclinic buserite at low pH. *American Mineralogist*, **85**, 826–838.

Lanson, B., Drits, V.A., Feng, Q., and Manceau, A. (2002) Structure of synthetic Na-birnessite: Evidence for a triclinic one-layer unit cell. *American Mineralogist*, **87**, 1662–1671.

Lee, J.S.K. and Huang, P.M. (1995) Photochemical effect on the abiotic transformations of polyphenolics as catalyzed by Mn(IV) oxide. Pp. 177–189 in: *Environmental Impact of Soil Component Interactions. Vol 1. Natural and Anthropogenic Organics* (P.M. Huang, J. Berthelin, J.-M. Bollag, W.B. McGill, and A.L. Page, editors). Lewis Publishers, Boca Raton, Florida, USA.

Li, L., Zhao, Z.Y., Huang, W.L., Peng, P., Sheng, G.Y., and Fu, J.M. (2004) Characterization of humic acids fractionated by ultrafiltration. *Organic Geochemistry*, **35**, 1025–1037.

Liu, C. and Huang, P.M. (2001) The influence of catechol humification on surface properties of metal oxides. Pp. 253–270 in: *Humic Substances: Structure, Models and Functions* (E.A. Ghabbour and G. Davies, editors). Royal Society of Chemistry, Cambridge, UK.

Liu, C. and Huang, P.M. (2002) Role of hydroxy-aluminosilicate ions (proto-imogolite sol) in the formation of humic substances. *Organic Geochemistry*, **33**, 295–305.

Liu, M.M., Zeng, Z.R., and Fang, H.F. (2005) Preparation and application of the sol-gel-derived acrylate/silicone co-polymer coatings for headspace solid-phase microextraction of 2-chloroethyl ethyl sulfide in soil. *Journal of Chromatography A*, **1076**, 16–26.

Majcher, E.H., Chorover, J., Bollag, J.M., and Huang, P.M. (2000) Evolution of CO$_2$ during birnessite-induced oxidation of C-14-labeled catechol. *Soil Science Society of America Journal*, **64**, 157–163.

Matocha, C.J. , Sparks, D.L., Amonette, J.E., and Kukkadapu, R.K. (2001) Kinetics and mechanism of birnessite reduction by catechol. *Soil Science Society of America Journal*, **65**, 58–66.

McBride, M.B. (1994) *Environmental Chemistry of Soils*. Oxford University Press, New York.

McKenzie, R.M. (1971) The synthesis of birnessite, cryptomelane, and some other oxides and hydroxides of manganese. *Mineralogical Magazine*, **38**, 493–502.

Nico, P.S. and Zasoski, R.J. (2000) Importance of Mn(III) availability on the rate of Cr(III) oxidation on δ-MnO$_2$. *Environmental Science & Technology*, **34**, 3363–3367.

Nico, P.S. and Zasoki, R.J. (2001) Mn(III) center availability as a rate controlling factor in the oxidation of phenol and sulfide on δ-MnO$_2$. *Environmental Science & Technology*, **35**, 3384–3343.

Potter, R.M. and Rossman, G.R. (1979) The tetravalent manganese oxides: identification, hydration, and structural relationships by infrared spectroscopy. *American Mineralogist*, **64**, 1199–1218.

Scheffer, F., Meyer, B., and Niederbudde, E. (1959) Huminstoflbildung unter katalyischer Einwirkung naturlich vorkornmender Eisenverbindungen im ModelIversuch. *Zeitschrift für Pflanzenernährung und Bodenkunde*, **87**, 26–44.

Shindo, H. and Huang, P.M. (1982) Role of manganese(IV) oxide in abiotic formation of humic substances in the

environment. *Nature*, **298**, 363−365.

Shindo, H. and Huang, P.M. (1985) The catalytic power of inorganic components in the abiotic synthesis of hydroquinone-derived humic polymers. *Applied Clay Science*, **1**, 71−81.

Shindo, H. and Huang, P.M. (1992) Comparison of the influence of Mn(IV) oxide and tyrosinase on the formation of humic substances in the environment. *Science of the Total Environment*, **117/118**, 103−110.

Stone, A.T. (1987) Reductive dissolution of manganese (III/IV) oxides by substituted phenols. *Environmental Science & Technology*, **21**, 979−986.

Tan, J.F., Qiu, G.H., Liu, F., Tan, W.F., and Feng, X.H. (2009) Effects of Mn (III) on oxidation of Cr (III) with birnessite. *Huanjing Kexue/Environmental Science (China)*, **30**, 2779−2785.

Tan, W., Koopal, L., Weng, L., Vanriemsdijk, W., and Norde, W. (2008) Humic acid protein complexation. *Geochimica et Cosmochimica Acta*, **72**, 2090−2099.

Villalobos, M., Toner, B., Bargar, J., and Sposito, G. (2003) Characterization of the manganese oxide produced by Pseudomonas putida strain MnB1. *Geochimica et Cosmochimica Acta*, **67**, 2649−2662.

Villalobos, M., Lanson, B., Manceau, A., Toner, B., and Sposito, G. (2006) Structural model for the biogenic Mn oxide produced by Pseudomonas putida. *American Mineralogist*, **91**, 489−502.

Wang, M.C. and Huang, P.M. (1992) Significance of Mn(IV) oxide in the abiotic ring cleavage of pyrogallol in natural environments. *Science of the Total Environment*, **113**, 147−157.

Wang, M.C. and Huang, P.M. (2000) Ring cleavage and oxidative transformation of pyrogallol catalyzed by Mn, Fe, Al, and Si oxides. *Soil Science*, **165**, 934−942.

Wang, M.C. and Huang, P.M. (2003) Cleavage and polycondensation of pyrogallol and glycine catalyzed by natural soil clays. *Geoderma*, **112**, 31−50.

Wang, M.C. and Huang, P.M. (2005) Cleavage of ^{14}C-labeled glycine and its polycondensation with pyrogallol as catalyzed by birnessite. *Geoderma*, **124**, 415−426.

Wilson, W.R. (1991) *Advances in Soil Organic Matter Research: The Impact on Agriculture and the Environment*. Royal Society of Chemistry, Cambridge, UK.

Zavarzina, A.G. (2006) A mineral support and biotic catalyst are essential in the formation of highly polymeric soil humic substances. *Eurasian Soil Science*, **39** (Suppl. 1), S48−S53.

Zhao, W., Feng, X., Tan, W., Liu, F., and Ding, S. (2009a) Relation of lead adsorption on birnessites with different average oxidation states of manganese and release of $Mn^{2+}/H^{+}/K^{+}$. *Journal of Environmental Sciences*, **21**, 520−526.

Zhao, W., Cui, H.J., Liu, F., Tan, W.F., and Feng, X.H. (2009b) Relation between Pb^{2+} adsorption and average Mn oxidation state in synthetic birnessites. *Clays and Clay Minerals*, **57**, 513−520.